PAPER • **OPEN ACCESS**

Folic acid-conjugated magnetic carbon nanotube nanocarriers for targeted delivery of mitoxantrone

OPEN ACCESS
IOP Publishing
Nanotechnology

Nanotechnology **36** (2025) 305701 (14pp)
https://doi.org/10.1088/1361-6528/aded95

Folic acid-conjugated magnetic carbon nanotube nanocarriers for targeted delivery of mitoxantrone

Buğçe Aydın[1,2], Serdar Bozoğlu[3], Nilgün Karatepe[3] and Fatma Seniha Güner[1,4,*]

[1] Department of Chemical Engineering, Istanbul Technical University, Istanbul 34469, Turkey
[2] Department of Chemical Engineering, Ondokuz Mayıs University, Samsun 55139, Turkey
[3] Energy Institute, Renewable Energy Division, Istanbul Technical University, Istanbul 34469, Turkey
[4] Sabancı University Nanotechnology Research and Application Center (SUNUM), Sabancı University, Istanbul 34956, Turkey

E-mail: guners@itu.edu.tr and seniha.guner@sabanciuniv.edu

Received 16 May 2025, revised 24 June 2025
Accepted for publication 9 July 2025
Published 22 July 2025

Abstract

Dual or multi-targeted delivery systems are a crucial aspect of optimal cancer treatment. These systems minimize side effects while maximizing therapeutic efficiency. With this motivation, in this study, we developed a dual-targeted nanocarrier system by modifying bovine serum albumin-coated magnetic carbon nanotubes (mCNT-BSA) with folic acid (FA) to enhance both magnetic and receptor-mediated targeting. The novel carrier was characterized using Fourier transform infrared spectroscopy, scanning electron microscopy-energy dispersive x-ray spectroscopy, x-ray photoelectron spectroscopy, vibrating sample magnetometer, and thermogravimetric analysis. Results confirmed successful FA conjugation and sufficient magnetic properties (14.7 emu g^{-1}) for external guidance. The system demonstrated a high mitoxantrone (MTO) loading capacity (120 μg mg^{-1}) and pH-sensitive release behavior, supporting drug release in acidic tumor microenvironments. *In vitro* cytotoxicity assays showed reduced toxicity of mCNT-BSA-FA/MTO on the MDA-MB-231 cancer cell line to free MTO. These findings suggest that mCNT-BSA-FA is a promising nanocarrier system for dual-targeted and controlled MTO delivery.

Keywords: folic acid, magnetic nanocarrier, mitoxantrone, single-walled carbon nanotubes, targeted drug delivery

* Author to whom any correspondence should be addressed.

1. Introduction

In recent years, an increasing number of people, younger or older, have been diagnosed with cancer. Despite significant advancements in conventional cancer treatments, managing the severe side effects remains a major challenge [1, 2]. Nanocarrier systems have been developed, which offer promising solutions to overcome these obstacles [3, 4].

Carbon nanotubes (CNTs) can be functionalized and decorated with a broad range of biological and chemical materials due to their remarkably active surface. Because of their needle-like structure and high tensile strength, CNTs have an obvious advantage over magnetic nanoparticles (mNPs) in that they can more readily pass through cell membranes and enter the bloodstream [5, 6]. Magnetic carbon nanotubes (mCNTs) are commonly sythesized by loading mNPs into the central cavity of CNTs or attaching mNPs to their surface. Due to their ability to enhance efficacy while reducing drug dosage and side effects, CNTs and mNPs can be combined to create highly functional hybrid magnetic systems. These systems hold great potential for the treatment of various diseases, including cancer or neurological disorders [7].

Mitoxantrone (MTO), a synthetic anthracenedione derivative anticancer agent, is commonly used in the treatment of breast, prostate, and leukemia [8, 9]. Unfortunately, MTO is nonspecific and has many side effects on healthy cells and tissues [10, 11]. Lately, targeted drug delivery nanosystems have emerged as a crucial approach for the treatment and diagnosis of cancers, aiming to reduce the toxicity of MTO [12, 13]. To achieve this, the surface of nanocarriers can be functionalized with various ligands that have the inherent ability to target tumor cells with overexpressed specific receptors [14, 15].

Many active targeting ligands have been conjugated to nanocarriers to enhance the selectivity of anticancer drugs for cancer cells. Among these ligands, folic acid (FA) is the most widely used targeting molecule because of its low cost, nontoxicity, and high stability [16]. Moreover, FA has a high binding affinity for the folate receptor (FR), which is overexpressed in many different types of cancer cells [17–19]. In numerous studies, an active targeting agent has been attached to the nanocarrier in addition to its magnetic feature to provide dual targeting properties [20–22]. These studies suggest that FA-conjugated magnetic nanocarrier systems have significant potential as anticancer agents.

Gholibegloo *et al* [21] prepared an FA-decorated magnetic cyclodextrin nanosponge for curcumin delivery. The *in-vitro* release studies and cytotoxicity assays exhibited a controlled drug release profile and selective cytotoxicity of the nanocarriers. Chen *et al* [23] developed FA-coated magnetic ordered mesoporous carbon nanospheres for the controlled release of doxorubicin (DOX). The drug carrier exhibited significant pH-sensitive release performance, with a DOX release rate of 22.5% at pH 5.6 and 5% at 7.4 over 30 h. The cytotoxicity of the FA-coated magnetic nanocarrier was both time-dependent and dose-dependent. In another study by Angelopoulou *et al* [24], FA-functionalized pegylated condensed mNPs were synthesized for DOX delivery. The nanocarrier exhibited enhanced uptake and cytotoxicity towards the MDA-MB-231 cells under a static magnetic field. In a study conducted by Rosa *et al* [25], magnetic multiwalled CNTs were functionalized with two different structures (a protein and a hydrophilic monomer), and the authors investigated the influence of an external magnetic field on the material's permeation in Caco-2 cells. In repeated tests under a magnetic field, exposing the material to magnets did not improve permeation. This highlights the importance of incorporating an active targeting agent, such as FA, alongside magnetic targeting to enhance the properties of the nanocarrier. To the best of our knowledge, there have been no study investigating the delivery of MTO utilizing a magnetic single-walled carbon nanotube (SWNT) nanocarrier coated with BSA and functionalized with FA.

In our previous study, we described BSA-coated mCNTs (mCNTs-BSA) using both covalent and noncovalent functionalization for MTO delivery [26]. Analyses demonstrated successful covalent modification of mCNT with BSA. Vibrating sample magnetometer (VSM) analysis proved that the magnetization value of mCNT-BSA was 15.6 emu g^{-1}, suggesting it can be magnetically guided to targeted sites. Further, mCNT-BSA had superparamagnetic properties, indicating its potential for targeted drug delivery. The results indicated that the BSA-coated nanocarrier is suitable for active targeting and has considerable potential for cancer treatment.

This study aims to develop an MTO-loaded nanocarrier system for more selective and efficient cancer treatment strategies by developing a dual-targeted drug delivery system that combines magnetic guidance with FR-mediated targeting. We hypothesize that the integration of mCNTs with BSA and FA will enable precise drug delivery to tumor sites, improving therapeutic outcomes while reducing systemic toxicity. By enhancing drug localization and pH-responsive release in acidic tumor environments, the nanocarrier has the potential to overcome the limitations of conventional chemotherapy. The proposed system could be further developed for personalized medicine applications and targeted delivery of various anticancer agents.

2. Materials and methods

2.1. Materials

Iron(III) chloride ($FeCl_3$), iron(II) sulfate heptahydrate ($FeSO_4.7H_2O$), ammonium hydroxide (NH_4OH), protocatechuic acid (PCA), bovine serum albumin (BSA), 1-ethyl-3-(3-(dimethylamino)propyl) carbodiimide (EDC), N-hydroxysuccinimide (NHS), folic acid (FA), tetrahydrofuran (THF; anhydrous, $\geqslant$99.9%), nitric acid (HNO_3; 65%), mitoxantrone dihydrochloride, and 3-(4,5-dimethylthiazol-2-yl)-2,5-diphenyltetrazolium bromide (MTT) were purchased from Sigma-Aldrich.

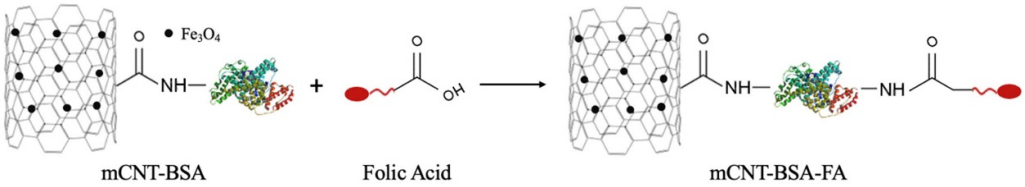

Figure 1. Schematic of the preparation of FA-conjugated mCNT-BSA.

2.2. Synthesis and stabilization of iron oxide nanoparticles (IONPs)

Synthesis of IONPs was carried out similarly to our previously reported study [26]. Briefly, 7.5 mmol of $FeCl_3$ and 7.5 mmol of $FeSO_4.7H_2O$ were dissolved in deionized water. 6.7 M ammonium hydroxide solution was added to the mixture to ensure a basic environment. The solution was stirred to precipitate the IONPs. IONPs were separated using a magnet and washed repeatedly with deionized water until the pH reached a neutral level. Finally, IONPs were dried in a vacuum oven at 65 °C.

PCA was used to coat the IONPs, providing them with colloidal stability in organic solvents. IONPs were added to an ammonium hydroxide solution adjusted to pH 12. After mixing with the mechanical stirrer, PCA was added to the solution. Stirring was continued at 1000 rpm for 15 min to allow for effective coating. The coated mNPs were separated using a magnet, washed with deionized water, and dried in a lyophilizer at −55 °C.

2.3. Synthesis and modification of single walled carbon nanotubes with IONPs

SWNTs were synthesized following the protocol described in our previous work and purified using 6 M HNO_3 solution [26]. The ligand exchange method was used to obtain mCNTs [27]. 1 g of SWNTs was dispersed in 20 ml of THF using an ultrasonic homogenizer for 30 min. Separately, 0.5 g of PCA-coated IONPs were dispersed in 15 ml of THF to form a second mixture, which was then added to the CNT dispersion. The mixture was stirred at 700 rpm for 6 h. Afterward, the mCNTs were separated using a magnet, washed with ethanol and deionized water, and dried in a vacuum oven at 50 °C.

2.4. Covalent functionalization of mCNTs with BSA

mCNT-BSA was synthesized according to our previously reported procedure [26]. Briefly, mCNTs were dispersed in phosphate buffered saline (PBS) solution using an ultrasonic bath. Subsequently, 75 mg of NHS and 125 mg of EDC were added to the mixture and stirred mechanically for 2 h in a dark room to activate the carboxyl groups. Then, 75 mg of BSA was added to the suspension. The coated nanocarriers were separated using a magnet and dried in a vacuum oven at 40 °C.

2.5. FA-conjugated mCNT-BSA

25 mg of FA was dissolved in 10 ml of PBS (pH 7.4), followed by continuous magnetic stirring for 2 h. After that, NHS (30 mg) and EDC (50 mg) were added to the solution in a 1:1 M ratio, and stirring was continued for an additional 2 h at room temperature. Separately, mCNT-BSA was added to 60 ml of PBS solution and dispersed using a mechanical stirrer for 2 h. The prepared FA solution was then added to the nanotube suspension, and the mixture was stirred in the dark for 24 h. FA-conjugated mCNT-BSA was separated using an external magnet, washed with distilled water, and dried in a vacuum oven at 40 °C. The conjugation of folic acid to the structure is illustrated in figure 1.

2.6. Characterization

Fourier transform infrared (FT-IR) spectroscopy was obtained using a PerkinElmer-Spectrum Two FT-IR/ATR instrument in the wavenumber range of 800–4000 cm^{-1}. Thermogravimetric analysis (TGA) was carried out using a thermogravimetric analyzer (Q600 SDT, TA Instruments) in a nitrogen atmosphere at a heating rate of 10 °C min^{-1}. VSM (Lake Shore 7407) was used to measure the magnetic properties of the nanocarriers at room temperature. The chemical composition of the samples was analyzed by x-ray photoelectron spectroscopy (XPS, Specs-Flex). The morphology of the samples was analyzed using a scanning electron microscope (SEM, JEOL-JSM7001F) equipped with an EDS. Transmission electron microscopy (TEM) images of samples were taken on a JEOL/JEM ARM 200 with an acceleration voltage of 200 kV. The sample was dispersed in ethanol for 30 min using an ultrasonic probe. It was then dripped onto the copper grid and dried overnight. The dispersions in water of mCNTs were also investigated. Nanocarriers with a concentration of 0.1 mg ml^{-1} were dispersed in distilled water and sonicated in an ultrasonic bath for 30 min. Then, the dispersion images were taken at 0, 1, 3, 24, 48 h, and 1 week.

2.7. MTO loading and release

For MTO loading studies, drug solutions containing 3 mg of mCNTs were prepared with a concentration of 0.1 mg ml^{-1}, in PBS adjusted to pH 9. The mixture was stirred in an orbital shaker at 25 °C for 48 h in the dark. To quantify the amount of unloaded MTO, the nanocarriers were washed twice with buffer solutions to eliminate any residual MTO. After mCNTs

were separated using a magnet, measurements were conducted at 611 nm with a UV–Vis spectrophotometer (Cary 60, Agilent Technologies). Concentration values were determined using the calibration curve established at pH 9. Drug loading efficiency and loading content were calculated using equations (1) and (2), respectively,

$$\text{Drug loading efficiency}\,(\%) = \frac{\text{mass of loaded MTO (mg)}}{\text{total MTO (mg)}} \times 100 \quad (1)$$

$$\text{Drug loading content} = \frac{\text{mass of loaded MTO } (\mu\text{g})}{\text{mass of nanocarrier (mg)}} \quad (2)$$

MTO release studies were performed in PBS at pH 5.5 and 7.4. For this purpose, 3 mg of MTO-loaded mCNTs was dispersed in 10 ml of PBS at 37 °C. At predetermined time intervals, samples were separated from the solution, and the MTO content was quantified using a UV–Vis spectrophotometer at 611 nm. Absorbance readings were converted into concentration values using calibration curves at pH 5.5 and 7.4. The cumulative drug release percentage was determined using equation (3),

$$\text{Cumulative release of MTO}\,(\%) = \frac{\text{mass of released MTO (mg)}}{\text{mass of MTO in nanocarrier (mg)}} \times 100 \quad (3)$$

2.8. Cell viability studies

The cytotoxic effects of FA-conjugated nanocarriers were evaluated on both normal and cancerous cell lines utilizing the MTT assay. Human embryonic kidney (HEK293T) and human breast cancer (MDA-MB-231) cell lines were selected for this study. For the MTT test, cells were seeded into 96-well plates at a density of 2500 cells per well. Then, cells were exposed to different concentrations of nanocarriers for 48 h. Following the incubation period, 5 mg ml^{-1} MTT reagent was added to each well. After a 4 h incubation, absorbance values were measured spectrophotometrically (BioTek 800 TS) at 570 nm. Untreated cells and culture medium were also tested as controls. Cell viability (%) was calculated relative to the control group. Additionally, cell studies involving MTO-loaded mCNT-BSA-FA on MDA-MB-231 cells were repeated with a magnet placed at the bottom of 96-well plates. To assess the targeting capability of the nanocarriers, MDA-MB-231 cells were pretreated with a 0.1 mg ml^{-1} free FA solution for 1 h prior to the addition of mCNT-BSA-FA/MTO. All experiments were conducted in triplicate. Absorbance data were analyzed using GraphPad Prism 7.0, and the results were compared with those of control cells. Cell images were captured using a Nikon Eclipse TS100 inverted microscope after 48 h of incubation.

2.9. Statistical analysis

Statistical analysis was performed using one-way analysis of variance (ANOVA) with Tukey's post-hoc test and Student's *t*-test. Differences were considered significant at $p \leqslant 0.05$. All results are expressed as the mean ± standard deviation.

3. Results

Since we focused on the conjugation of FA with mCNT-BSA in this study, the synthesis and characterization data of mCNT and mCNT-BSA, which were our main aim in our previous study [26], are briefly discussed below. This section mainly addresses the conjugation and characterization of folic acid, as well as studies on drug loading and release.

3.1. Synthesis of mCNT and mCNT-BSA

In our previous study, we characterized mCNT and mCNT-BSA using Raman spectroscopy, FT-IR, TGA, scanning electron microscopy-energy dispersive x-ray spectroscopy (SEM-EDS), XPS, and VSM analyses [26]. In addition to these characterization methods, TEM images of mCNTs and mCNT-BSA are presented in figure 2. As shown in figures 2(a) and (b), the CNTs and magnetite exhibit tubular and spherical shapes, respectively. It is noted that CNTs have diameters ranging between 10 and 20 nm. In figures 2(c) and (d), bright and dark regions indicate the presence of BSA and stacks of Fe_3O_4 nanoparticles attached to the CNTs.

3.2. Characterization of mCNT-BSA-FA

The surface morphology and successful conjugation of folic acid onto mCNT-BSA were analyzed using FT-IR, TGA, XPS, and SEM-EDS.

FT-IR spectroscopy was employed to identify functional groups in the mCNTs. The FT-IR spectra of mCNT-BSA-FA and FA are shown in figure 3(a) [28]. The specific peaks that belong to the functional groups are given in table 1. The peaks of mCNT-BSA at 1643 cm^{-1} (amide I), 1533 cm^{-1} (amide II), 1394 cm^{-1} (amide III), and 1100 cm^{-1} (±10) (C–O) were shifted to 1645 cm^{-1}, 1530 cm^{-1}, 1388 cm^{-1}, and 1084 cm^{-1} (±10) positions, respectively, in the mCNT-BSA-FA spectra [19, 26, 29, 30]. New peaks observed at 1449 and 1157 cm^{-1} (±10) in the mCNT-BSA-FA spectrum are associated with the phenyl and nitrogenous heterocyclic rings of folic acid, respectively [23, 31]. Slight shifts in the peaks are in close agreement with the previous studies and confirm the FA-conjugation [29, 30].

TGA was used to determine the weight losses of nanocarriers in a nitrogen atmosphere. As depicted in figure 3(b), the thermal degradation of folic acid occurs in four stages. In the first stage (100 °C–150 °C), adsorbed water is removed, while in the second stage (200 °C–350 °C), glutamic acid is eliminated. The third stage (380 °C–450 °C) shows weight loss associated with the degradation of functional groups in folic acid, such as pterin and p-aminobenzoic acid. The fourth stage (650 °C–750 °C) corresponds to the formation of pyrolysis products [32]. The total weight loss of mCNT-BSA-FA upon heating to 900 °C is 25.0 ± 0.1%. In this temperature range, BSA and FA are removed from the structure [33, 34].

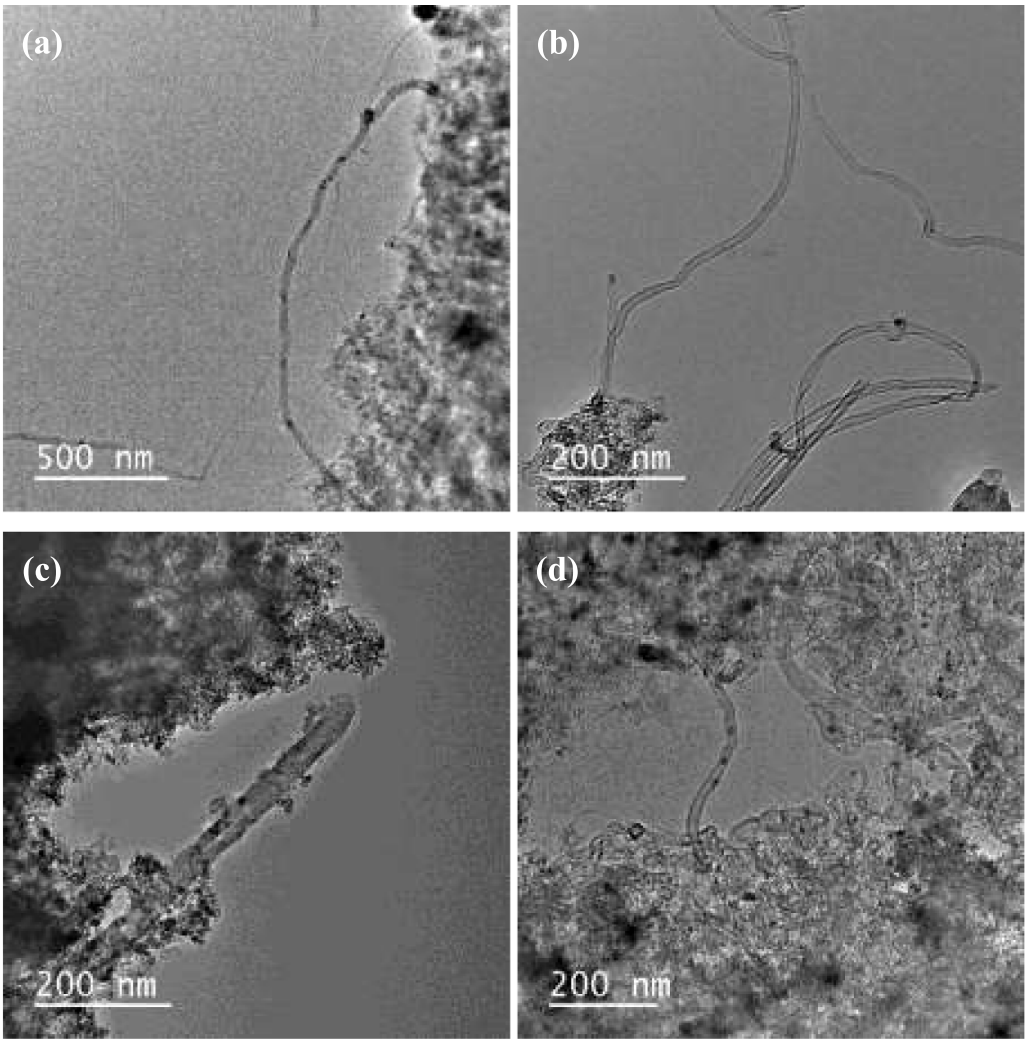

Figure 2. TEM images of synthesized (a), (b) mCNT, and (c), (d) mCNT-BSA.

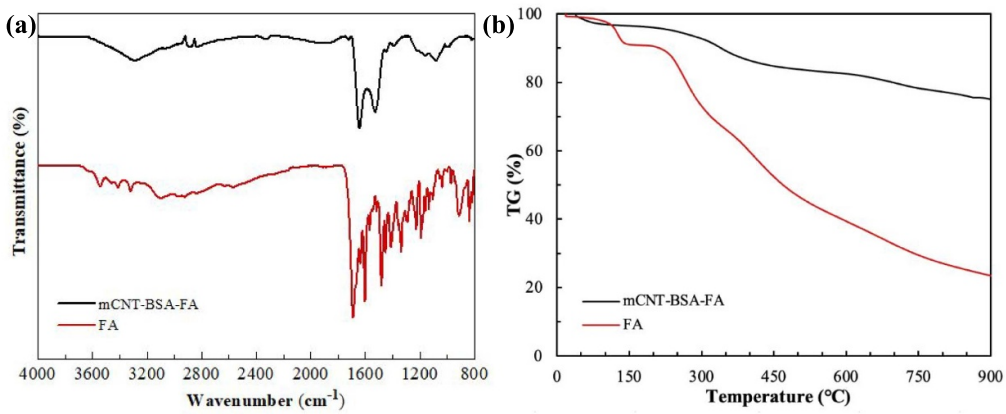

Figure 3. (a) FT-IR spectra, and (b) TGA curves of mCNT and mCNT-BSA-FA.

The morphological structure of mCNT-BSA-FA was investigated by SEM analysis (figure 4(a)), and the atomic percentages of the elements in the nanocarrier were determined using EDS (figure 4(b)). The results show that the percentages of C, O, Fe, and S for mCNT-BSA and mCNT-BSA-FA are 76.08%, 14.48%, 8.23%, 0.95%; and 78.17%, 14.12%, 6.80%, 0.52%, respectively. The percentages of Fe and S decreased after the nanocarrier was functionalized with folic acid, compared to the EDS result of mCNT-BSA [35, 36]. Nevertheless, nitrogen was not detected, likely due to its low content in the

Table 1. FT-IR analysis of mCNT-BSA-FA and FA.

Sample	IR band (cm^{-1})	Functional group
mCNT-BSA-FA	1645 (±10)	C=O (amide I)
	1530 (±10)	C–N, N–H (amide II)
	1449 (±10)	Phenyl ring
	1388 (±10)	C–N (amide III)
	1157 (±10)	Nitrogenous heterocyclic ring
	1084 (±10)	C–O
	1004 (±10)	O–H, C–O
Folic Acid	3100 (±10)	O–H
	1691 (±10)	C=O (–COOH)
	1637 (±10)	C=O, C–N (–$CONH_2$)
	1604 (±10)	C=C, N–H
	1483 (±10)	C=C, phenyl ring
	1160 (±10)	Nitrogenous heterocyclic ring

nanocarrier. The N content in the sample was determined using XPS analysis.

In addition to the SEM analysis, the surface elemental composition of mCNT-BSA-FA was characterized using XPS analysis (figure 5(a)). FA mainly consists of nitrogen, oxygen, and carbon. As depicted in figure 5(a), mCNT-BSA-FA contains carbon, oxygen, nitrogen, sulfur and iron. Sulfur originates solely from BSA, while nitrogen is derived from both BSA and FA [37]. Following FA conjugation to mCNT-BSA, the XPS spectrum displays peaks for C 1s, O 1s, N 1s, S 1s and Fe 2p at about 285 eV, 531 eV, 400 eV, 164 eV, and 710 eV, respectively. The atomic percentage of N for mCNT-BSA was found to be 9.4%, while this value increased to 10.2% for mCNT-BSA-FA [26]. The sulfur content was determined to be 0.4%, which is the same as that of the BSA-coated nanocarrier. The XPS analysis confirmed the successful grafting of FA onto the surface of mCNT-BSA.

The magnetization curve of mCNT-BSA-FA was shown from −20 to +20 kOe at room temperature in figure 5(b). The saturation magnetization (*Ms*) value of the FA-conjugated nanocarrier was measured as 14.7 emu g^{-1}. This value is lower than *Ms* of mCNT (16.8 emu g^{-1}) and mCNT-BSA (15.6 emu g^{-1}) due to the existence of nonmagnetic coatings on the surface of mCNTs [26, 36, 38]. Moreover, the hysteresis loop (<20 Oe) was not observed in the magnetization curve, which exhibited the superparamagnetic property of the nanocarrier [39, 40].

Due to their morphology and hydrophobic structure, CNTs tend to cluster and form bundles under the influence of van der Waals forces. However, the introduction of the –COOH and –OH groups on the surface of CNTs can increase their solubility and dispersion [41]. The dispersions of mCNT, mCNT-BSA, and mCNT-BSA-FA in water were investigated by taking photographs at 1, 3, 24, 48 h and 1 week and compared to their initial state (figure 6). At the end of 1 week, it was observed that the distribution of mCNT was stable due to the presence of oxygen-containing groups. After the conjugation of Fe_3O_4 nanoparticles to CNTs, the surface tension and aggregation of CNTs decrease due to the steric barrier effect of Fe_3O_4 [42, 43]. Figure 6 illustrates that nanoparticle agglomeration increased significantly after BSA coating. The stability was markedly enhanced after mCNT-BSA was functionalized with FA. This indicates that BSA alone was not effective in improving mCNT stability, and gravitational forces are effective in mCNT-BSA. Notably, FA made a substantial contribution to enhancing nanocarrier dispersion.

3.3. MTO loading and release

In this study, MTO, a widely used cancer treatment drug, was chosen as the model drug. The loading of MTO onto nanocarriers is mainly facilitated by π–π stacking and electrostatic attraction due to its aromatic nature. After 48 h of loading, the MTO loading efficiency and loading content for mCNT-BSA-FA were determined as 35.9% and 120 $\mu g\ mg^{-1}$, respectively. Functionalizing nanocarriers with organic structures such as folic acid can reduce the MTO loading capacity. MTO loading efficiency and MTO content of mCNT-BSA were found to be 43.4% and 145 $\mu g\ mg^{-1}$, respectively [26]. This result is attributed to a decrease in the available region for π–π interactions between the nanotube and drug molecules [44].

The MTO release profile depicted in figure 7 suggests a high initial release within the first 1 h, followed by a sustained release at both different pHs from the nanocarrier. Upon functionalization of mCNT-BSA with FA, mCNT-BSA-FA exhibited an distinct pH-sensitive MTO release pattern. MTO release for pH 5.5 (lysosomal) and 7.4 (physiological) was found to be 68.6% and 49.9%, respectively. In an acidic environment, the amine groups of MTO molecules become protonated, decreasing hydrophobic interactions between MTO molecules and mCNT, thus accelerating MTO release [13, 45, 46]. Moreover, mCNT-BSA-FA showed a slightly faster MTO release compared to FA-free nanocarriers due to its improved dispersibility [26]. In our study, MTO release from the mCNT-BSA was determined to be 36.8% and 44.1% at pH 5.5 in the first 1 and 6 h, respectively, while it was 55.3% and 64.3% for the FA-coated nanocarrier.

3.4. MTO release kinetics

Kinetic model equations were applied to assess the release mechanism of MTO from mCNT-BSA-FA over the first 24 h. All parameters in these equations, including the coefficient of determination (R^2), empirical parameters, and constants are summarized in table 2. According to the R^2 value, the *in vitro* MTO release data best fit the Korsmeyer–Peppas equation at both acidic and neutral pH. The most critical characteristic of the model is its exponential value (n). Based on the Korsmeyer-Peppas model, the n values for MTO release were found to be 0.0593 and 0.0724 at pH 5.5 and 7.4, respectively. These results suggested that the MTO release from mCNT-BSA-FA is controlled by Fickian diffusion ($n < 0.45$) [19, 41]. Moreover, the k_P value at pH 5.5 is higher than that at 7.4, indicating that the MTO release rate is greater in an acidic environment [22].

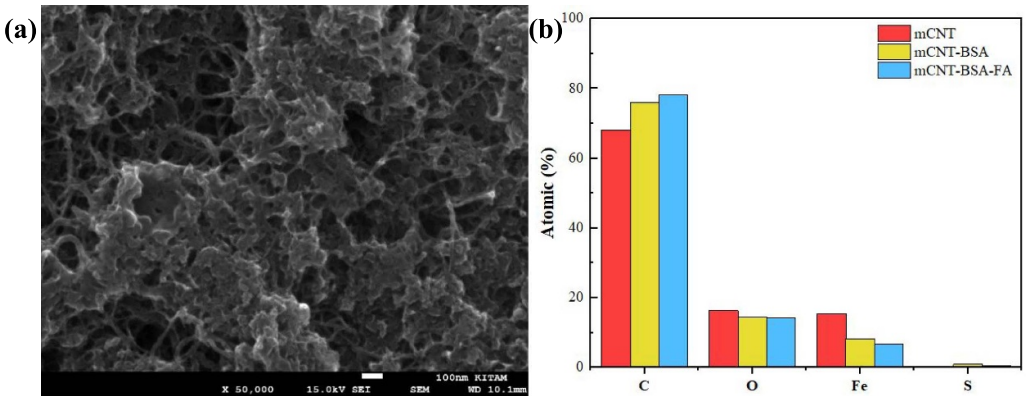

Figure 4. (a) SEM image of mCNT-BSA-FA, and (b) EDS results of uncoated and coated mCNTs.

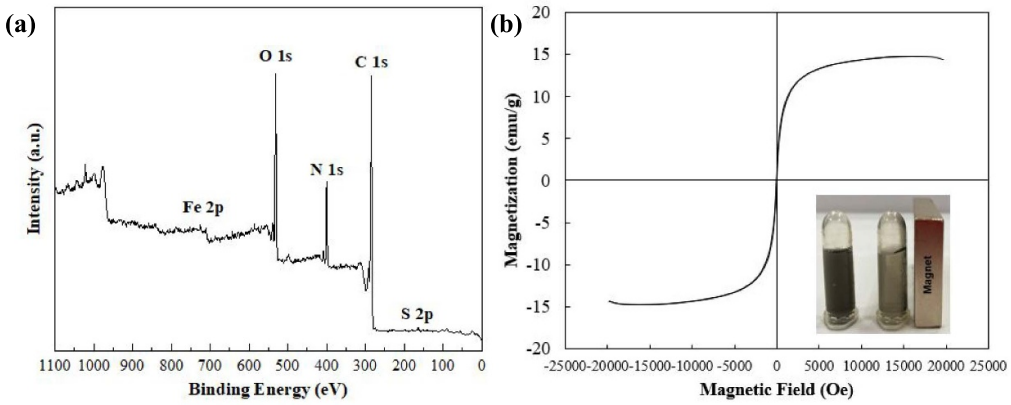

Figure 5. (a) XPS spectrum, and (b) magnetization curve of mCNT-BSA-FA. The inset illustrates the behavior of mCNT-BSA-FA dispersed in water under the influence of a magnetic field.

3.5. In-vitro *cytotoxicity studies*

The cytotoxicity of FA-functionalized mCNT-BSA was evaluated using an MTT assay on HEK293T cell lines. HEK293T cells were treated with nanocarriers in the concentration range of 5–50 μg ml^{-1} (figure 8(a)). A clear decrease in cell viability (%) was observed as the concentration of nanocarriers increased, likely due to increased aggregation at higher nanoparticle concentrations. For cytotoxicity tests, the dispersibility of nanocarrier systems is a crucial parameter. Functionalization with FA improved the dispersion of the nanocarriers. In addition, statistical analysis showed a significant difference ($p < 0.05$) in cell viability between mCNT-BSA-FAs and the control group.

The cytotoxic effects of MTO-loaded mCNT-BSA-FA at various concentrations (5, 10, 25, and 50 μg ml^{-1}) on the viability of MDA-MB-231 cells are given in figure 8(b). As expected, cell viability reduced with increasing nanocarrier concentration due to the higher exposure of cells to MTO.

Figure 9 shows the cell viability of MDA-MB-231 cells treated with free MTO and both MTO-loaded and unloaded nanocarriers at concentrations of 5 and 25 μg ml^{-1}. It was observed that increasing the concentration of mCNT-BSA-FA from 5 to 25 μg ml^{-1} resulted in greater cytotoxicity in the cell line ($p < 0.05$). Furthermore, when comparing the cell viability (%) of nanocarriers with and without FA on MDA-MB-231, cell viability was determined to be 60% and 32% for mCNT-BSA/MTO and mCNT-BSA-FA/MTO at a concentration of 5 μg ml^{-1}, respectively [26]. This result indicates that the strong binding affinity of FA to its receptor plays a significant role in improving the selectivity of the carrier system which is attributed to its receptor-mediated endocytosis [20, 47].

After 48 h of treatment, it was observed that the cell viability (%) of mCNT-BSA-FA/MTO was slightly higher than that of free MTO ($p < 0.05$) at the same MTO concentration (figure 9). This result may be attributed to the cumulative release of MTO from mCNT-BSA-FA, which is 68.6% at pH 5.5 after 48 h (figure 7). On the contrary, the amount of free MTO is higher than that of MTO released from mCNT-BSA-FA/MTO. The critical cytotoxicity appears to result from MTO released from nanocarriers compared to unloaded nanocarriers. Free MTO rapidly accumulates in the cells through passive diffusion and can also damage healthy tissues, limiting the clinical applications of the chemotherapeutic agent. However, cancer agents delivered via nanocarrier systems

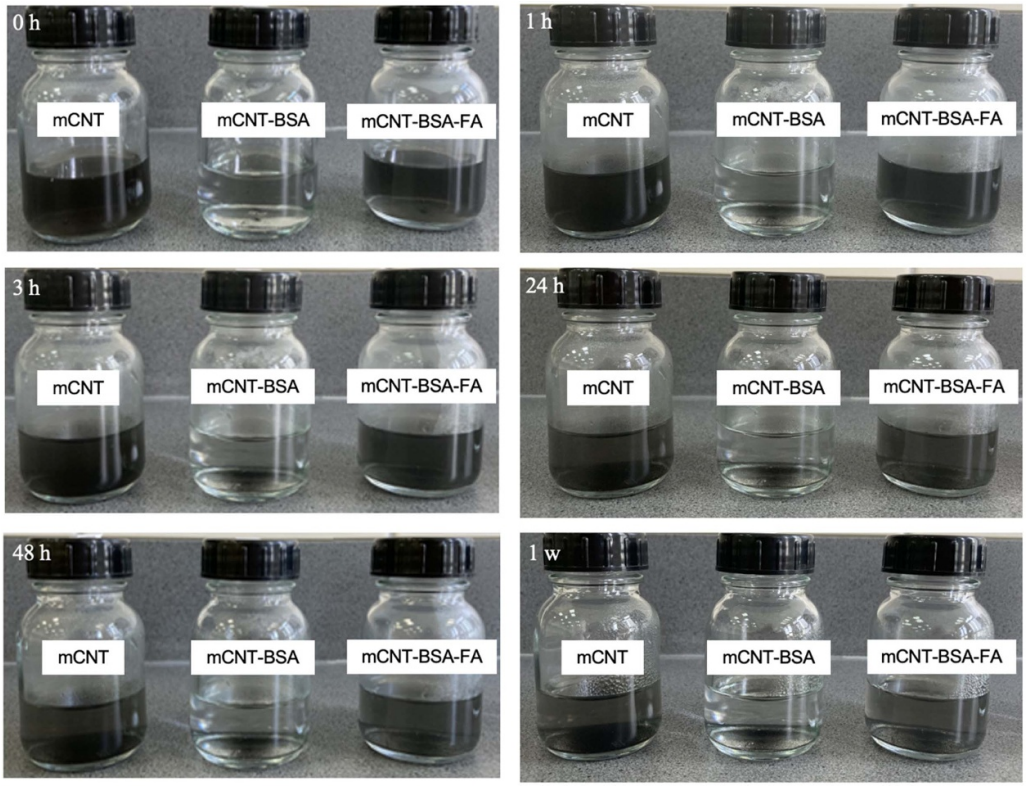

Figure 6. Dispersion of nanocarriers in water.

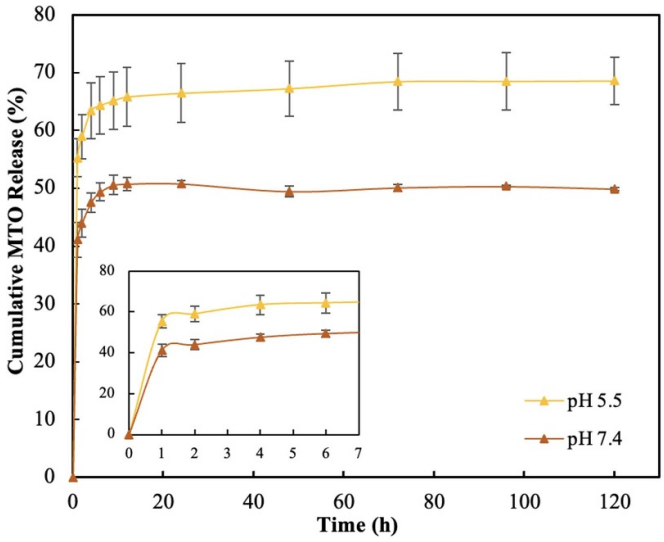

Figure 7. MTO release profile of mCNT-BSA-FA for pH 5.5 and 7.4 (inset: release within the first 6 h).

exhibit time-dependent release at the target site before interacting with cells. While the free drug exhibits higher cytotoxicity in the cells at the same concentration, nanocarrier systems require specific conditions and time to release the drug [48, 49].

Furthermore, the cytotoxic effects of different concentrations of FA solutions used to block FRs were examined. When incubated with FA solutions, cell viability decreased with increasing FA concentration, indicating a dose-dependent response (figure 10). No significant difference was observed between the folic acid solution at a 0.1 mg ml^{-1} concentration and the control group.

Blocking FRs and repeating the tests in the presence of a magnet did not result in a significant difference ($p > 0.05$) between the groups (figure 9). Shi *et al* [50] investigated the cytotoxicity of deoxycholic acid, PEG, and FA-modified chitosan for doxorubicin delivery on HeLa cells, reporting a cytotoxicity profile similar to that observed in our present

Table 2. Kinetic model data for MTO release from mCNT-BSA-FA.

			mCNT-BSA-FA	
Kinetic models	Equation	Parameters	pH 5.5	pH 7.4
Zero-order	$\frac{M_t}{M_\infty} = k_0\, t$	k_0	0.3802	0.3467
		R^2	0.5335	0.5169
First-order	$\log\left(1 - \frac{M_t}{M_\infty}\right) = \frac{k_1 t}{2.303}$	k_1	0.0101	0.0064
		R^2	0.5608	0.5287
Higuchi	$\frac{M_t}{M_\infty} = k_H t^{0.5}$	k_H	2.6565	2.4482
		R^2	0.7275	0.7196
Korsmeyer–Peppas	$\log \frac{M_t}{M_\infty} = \log k_P + n \log t$	k_P	56.715	42.141
		n	0.0593	0.0724
		R^2	0.8966	0.8948

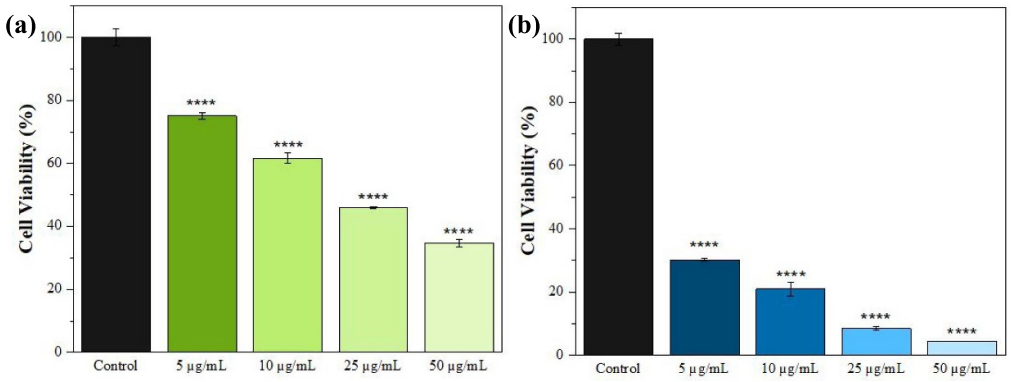

Figure 8. Cell viability results for (a) mCNT-BSA-FA on HEK293T and (b) mCNT-BSA-FA/MTO on MDA-MB-231 cells. Data are represented as the mean ± SD ($n = 3$). One-way analysis of variance (ANOVA) with Tukey posthoc test; **** $p < 0.0001$ compared with the control group.

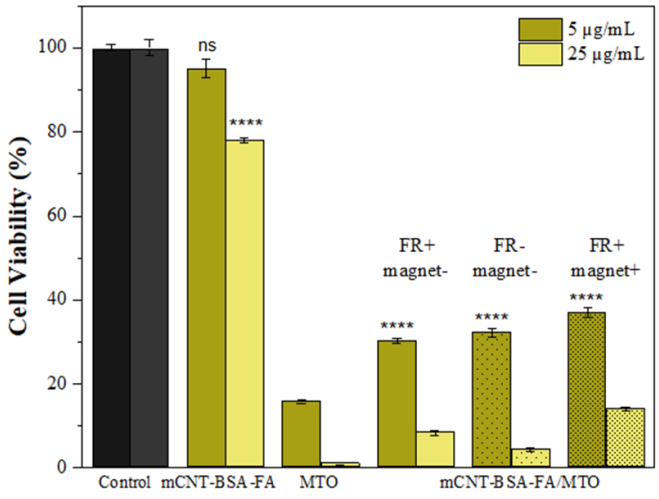

Figure 9. Cell viability results for free MTO, MTO-loaded and unloaded nanocarriers at concentrations of 5 and 25 μg ml^{-1} on MDA-MB-231 under different conditions. FR+: folate receptor positive, FR-: folate receptor negative, magnet-: without a magnet, and magnet+: with a magnet. Data are represented as the mean ± SD ($n = 3$). One-way analysis of variance (ANOVA) with Tukey posthoc test; ns indicates not significant and **** $p < 0.0001$ for mCNT-BSA-FA vs control group and mCNT-BSA-FA/MTO vs MTO.

study. At applied nanocarrier concentrations (0.1, 1 and 40 μg ml^{-1}), there was no significant difference in cell viability between treatments with and without the free FA solution.

Figure 11 represents inverted microscope images of MDA-MB-231 cells after treatment with mCNT, mCNT-BSA, and mCNT-BSA-FA/MTO at a concentration of 5 μg ml^{-1} for

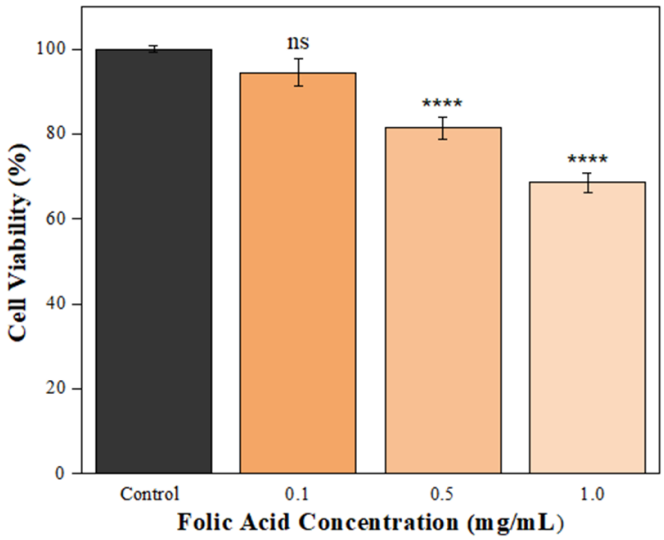

Figure 10. Cell viability results of folic acid solutions on MDA-MB-231 cells. Data are represented as the mean ± SD ($n = 3$). One-way analysis of variance (ANOVA) with Tukey posthoc test; ns indicates not significant and **** $p < 0.0001$ compared with the control group.

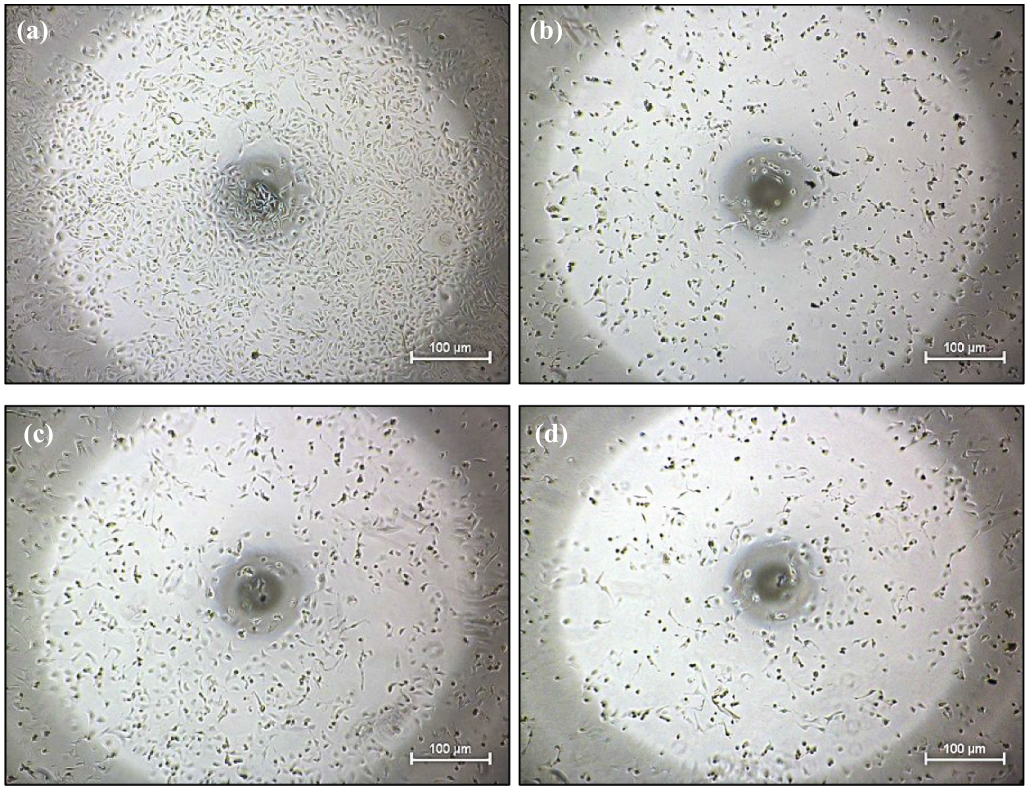

Figure 11. Cell morphology of MDA-MB-231 cells treated with 5 μg ml^{-1} of nanocarriers: (a) control, (b) mCNT/MTO, (c) mCNT-BSA/MTO, and (d) mCNT-BSA-FA/MTO.

48 h. As depicted in figure 11(a), MDA–MB–231 cells exhibit elongated spindle-shaped morphology. The MTO-loaded mCNTs induced significant morphological changes; most of the cells underwent shrinkage and loss of their typical morphology. Treated cells displayed notable morphological alterations compared to untreated cells, indicating the cytotoxic effects of the nanocarriers. Consistent with the MTT assay results [26], fewer cells were observed after 48 h of incubation than in the control group. Figures 11(b)–(d) depict gaps between MDA-MB-231 cells; unlike the control group, and an apparent reduction in cell volume and shrinkage was observed.

Table 3. Comparison of reported carbon-based nanocarriers functionalized with folic acid for targeted treatment.

Nanocarrier	Coating	Drug	Loading efficiency (%)	Inferences	References
Graphene quantum dots	PEG	Mitoxantrone	97.5	FA-PEG conjugation reduced cell viability on HeLa (FR+).	[14]
Graphene oxide	BSA	Doxorubicin	—	The FA-conjugated nanocarrier exhibited significant inhibition of MCF7 (FR+) cells.	[29]
Graphene oxide	PEG	Camptothecin	45	FA-PEG functionalized GO showed higher cytotoxicity to MCF7 cells.	[57]
CNT	PEG	Raloxifene	71	The FA-conjugated nanocarrier entered MCF7 cells via endocytosis.	[58]
CNT	Sodium alginate, chitosan	Doxorubicin	—	Folic acid facilitated receptor-mediated internalization, and the nanocarrier had a more cytotoxic effect compared to free DOX on HeLa cells.	[59]
mCNT	Polyacrylic acid	Doxorubicin	∼95	When FR was blocked, reduced cellular internalization was observed in U87 cells.	[60]
mCNT	BSA	Mitoxantrone	43.4	Cytotoxicity decreased compared to free MTO. Cell viability in MDA-MB-231 (FR+) cells was reduced compared to the FA-free nanocarrier.	Present study

4. Discussion

Magnetic stimuli systems offer several advantages for targeted drug delivery, including ease of application, potential for remote control, and hyperthermia effect at the targeted site. These characteristics make magnetic-triggered systems a promising approach for the development of targeted drug delivery systems with enhanced therapeutic efficacy and reduced side effects [51]. Ligand binding or stimulating systems operate based on different mechanisms and have distinct characteristics. Attaching a ligand to a nanocarrier is a commonly employed strategy to enhance its specificity for targeting particular cells or tissues. These ligands exhibit selectivity for receptors that are overexpressed in tumor region, enabling the nanocarriers to accumulate specifically in this region [52–54].

This study aimed to develop a dual-targeted drug delivery system for cancer treatment by functionalizing mCNT-BSA with FA through covalent modification. The successful conjugation of mCNT-BSA was confirmed using several analysis techniques, including FT-IR spectroscopy, XPS, TGA, VSM and SEM-EDS. Moreover, MTO loading/release and cell viability tests of FA-conjugated nanoparticles were conducted.

In the EDS analysis, after FA conjugation, the percentages of iron and sulfur decreased from 8.23% to 6.80% and from 0.95% to 0.52%, respectively. Similarly, in the XPS analysis, an increase in nitrogen content from 9.4% to 10.2% was observed, confirming the presence of FA. VSM analysis revealed that the magnetization value of the nanocarrier was 14.7 emu g^{-1}, demonstrating its ability to be magnetically directed to tumor sites. The loading efficiency and loading content of MTO of mCNT-BSA-FA were determined to be 35.9% and 120 μg mg^{-1}, respectively. Additionally, we found that FA enhanced the stability and pH-sensitive release properties of the nanocarrier. The pH-sensitive characteristics can facilitate the targeted delivery of anticancer drugs by improving therapeutic efficiency and minimizing side effects, given that cancer cells typically exhibit a lower pH than healthy cells.

The MTO release studies revealed that drug release significantly increased following the functionalization of the nanocarriers, supported by kinetic model analyses. The results are consistent with previously published studies. Dinan *et al* [44] demonstrated that polyethylene glycol (PEG) and FA-coated CNTs were effective for doxorubicin delivery. While the drug release of CNT at pH 5 was 15.26%, it increased to 42.50% and 54.40%, respectively, after coating with PEG and FA. Moreover, the positive effects of functionalized nanocarriers on the viability of normal cells are documented in previously published studies [55, 56]. In a study by Akbar *et al* [48], a folic acid and chitosan-coated metal organic framework was designed for 5-fluorouracil delivery. When evaluating the toxic effects of drug-loaded nanocarriers on the HEK293 cell

line, it was found that cell viability (%) increased after functionalization with FA and chitosan. Specifically, while the cell viability of the pristine nanocarriers was approximately 35% at a concentration of 500 μg ml^{-1}, it increased to approximately 70% after functionalization.

In table 3, some nanocarriers conjugated with FA for targeted delivery systems are compared with reported carbon-based carriers, summarizing their drug loading behavior and cytotoxicity effect on cancerous cell lines. According to table 3, mCNT-BSA-FA demonstrates acceptable performance in enhancing the cytotoxic effect of the nanocarrier on FR+ cells and can be regarded as a significant carrier for targeted delivery systems.

Experimental results showed that free MTO had a higher cytotoxic effect than mCNT-BSA-FA/MTO on the MDA-MB-231 cancer cell line. The nanocarrier system we designed incorporates not only pH- and magnetically-responsive stimuli but also an active targeting ligand. This enables the drug to be released preferentially in cancerous tissues rather than in healthy cells, potentially overcoming the limitations of conventional cancer treatments. Therefore, the nanocarrier system attracts attention as a promising drug delivery system for enhancing the therapeutic efficacy of the MTO. However, a major limitation of this study is the lack of *in vivo* evaluation of the nanocarrier system. Future studies should be expanded to include toxicity profiles and therapeutic efficacy *in vivo*. Nevertheless, this study highlights the potential of dual-targeting techniques to achieve synergistic enhancements in smart drug delivery applications.

5. Conclusions

Novel folic acid-conjugated mCNTs were prepared for the controlled and targeted delivery of MTO. Characterization results of mCNT-BSA-FA indicated that the nanocarriers possessed sufficient magnetization for separation and guidance via an external magnet. The superparamagnetic properties of these nanocarrier systems are important for effective drug delivery. Comparison of photographs showing dispersion in water revealed that mCNT-BSA-FA exhibited superior stability. mCNT-BSA-FA/MTO demonstrated a drug release of 49.9% at physiological pH, whereas 68.6% drug release was observed at acidic pH conditions. Cytotoxicity investigations of FA-conjugated nanotubes were conducted on HEK293T and MDA-MB-231 cell lines, demonstrating dose-dependent cytotoxicity. Considering the pH-sensitive release and excellent dispersion properties of MTO-loaded mCNT-BSA-FA, it emerges as a promising candidate for drug delivery applications.

Data availability statement

All data that support the findings of this study are included within the article (and any supplementary files).

Acknowledgments

This work was supported by the Istanbul Technical University Scientific Research Projects Foundation (Project No: MDK-2020-42751).

Author contributions

Buğçe Aydın 0000-0001-5104-1484
Data curation (lead), Investigation (equal), Methodology (equal), Visualization (lead), Writing – original draft (lead)

Serdar Bozoğlu 0000-0001-7653-3506
Investigation (equal), Methodology (equal), Writing – original draft (supporting)

Nilgün Karatepe 0000-0002-7392-4103
Resources (equal), Supervision (equal)

Fatma Seniha Güner 0000-0002-3414-4868
Conceptualization (lead), Project administration (lead), Resources (equal), Supervision (equal), Writing – review & editing (lead)

References

[1] Hosnedlova B, Kepinska M, Fernandez C, Peng Q, Ruttkay-Nedecky B, Milnerowicz H and Kizek R 2019 Carbon nanomaterials for targeted cancer therapy drugs: a critical review *Chem. Rec.* **19** 502–22
[2] Kumari P, Ghosh B and Biswas S 2016 Nanocarriers for cancer-targeted drug delivery *J. Drug Target.* **24** 179–91
[3] Chen Z, Zhang A, Wang X, Zhu J, Fan Y, Yu H and Yang Z 2017 The advances of carbon nanotubes in cancer diagnostics and therapeutics *J. Nanomater.* **2017** 1–13
[4] Sahu T, Ratre Y K, Chauhan S, Bhaskar L V K S, Nair M P and Verma H K 2021 Nanotechnology based drug delivery system: current strategies and emerging therapeutic potential for medical science *J. Drug Deliv. Sci. Technol.* **63** 102487
[5] Samadishadlou M, Farshbaf M, Annabi N, Kavetskyy T, Khalilov R, Saghfi S, Akbarzadeh A and Mousavi S 2018 Magnetic carbon nanotubes: preparation, physical properties, and applications in biomedicine *Artif. Cells, Nanomed. Biotechnol.* **46** 1314–30
[6] Raphey V R, Henna T K, Nivitha K P, Mufeedha P, Sabu C and Pramod K 2019 Advanced biomedical applications of carbon nanotube *Mater. Sci. Eng. C* **100** 616–30
[7] Stopin A and Bonifazi D 2021 *Biological Applications of Magnetically Empowered Carbon Nanotubes* (Royal Society of Chemistry)
[8] Wani A, Muthuswamy E, Savithra G H L, Mao G, Brock S and Oupický D 2012 Surface functionalization of mesoporous silica nanoparticles controls loading and release behavior of mitoxantrone *Pharma. Res.* **29** 2407–18
[9] Risi G, Bloise N, Merli D, Icaro-Cornaglia A, Profumo A, Fagnoni M, Quartarone E, Imbriani M and Visai L 2014 Invitro study of multiwall carbon nanotubes (MWCNTs) with adsorbed mitoxantrone (MTO) as a drug delivery system to treat breast cancer *RSC Adv.* **4** 18683–93
[10] Sargazi A, Shiri F, Keikha S and Majd M H 2018 Hyaluronan magnetic nanoparticle for mitoxantrone delivery toward CD44-positive cancer cells *Colloids Surf. B* **171** 150–8

[11] Lam P, Lin R D and Steinmetz N F 2018 Delivery of mitoxantrone using a plant virus-based nanoparticle for the treatment of glioblastomas *J. Mater. Chem. B* **6** 5888–95
[12] Singh A, Bora S, Khurana S, Kumar P, Sarkar N, Kukreti R, Kukreti S and Kaushik M 2023 Advance nanotherapeutic approach for systemic co-delivery of mitoxantrone loaded chitosan coated PLGA nanoparticles to improve the chemotherapy against human non-small cell lung cancer *J. Drug Deliv. Sci. Technol.* **84** 104523
[13] Wang J, Asghar S, Jin X, Chen Z, Huang L, Ping Q, Zong L and Xiao Y 2018 Mitoxantrone-loaded chitosan/hyaluronate polyelectrolyte nanoparticles decorated with amphiphilic PEG derivates for long-circulating effect *Colloids Surf. B* **171** 468–77
[14] Li Z, Fan J, Tong C, Zhou H, Wang W, Li B, Liu B and Wang W 2019 A smart drug-delivery nanosystem based on carboxylated graphene quantum dots for tumor-targeted chemotherapy Nanomedicine *Nanomedicine* **14** 2011–25
[15] Granja A, Nunes C, Sousa C T and Reis S 2022 Folate receptor-mediated delivery of mitoxantrone-loaded solid lipid nanoparticles to breast cancer cells *Biomed. Pharmacother.* **154** 113525
[16] Mahajan S, Patharkar A, Kuche K, Maheshwari R, Deb P K, Kalia K and Tekade R K 2018 Functionalized carbon nanotubes as emerging delivery system for the treatment of cancer *Int. J.Pharm.* **548** 540–58
[17] Barar J, Kafil V, Majd M H, Barzegari A, Khani S, Johari-Ahar M, Asgari D, Cokous G and Omidi Y 2015 Multifunctional mitoxantrone-conjugated magnetic nanosystem for targeted therapy of folate receptor-overexpressing malignant cells *J. Nanobiotechnol.* **13** 1–16
[18] Tonbul H, Sahin A, Tavukcuoglu E, Ultav G, Akbas S, Aktas Y, Esendaglı G and Capan Y 2021 Folic acid decoration of mesoporous silica nanoparticles to increase cellular uptake and cytotoxic activity of doxorubicin in human breast cancer cells *J. Drug Deliv. Sci. Technol.* **63** 102535
[19] Anirudhan T S and Christa J 2018 pH and magnetic field sensitive folic acid conjugated protein–polyelectrolyte complex for the controlled and targeted delivery of 5-fluorouracil *J. Ind. Eng. Chem.* **57** 199–207
[20] Avedian N, Zaaeri F, Daryasari M P, Akbari Javar H and Khoobi M 2018 pH-sensitive biocompatible mesoporous magnetic nanoparticles labeled with folic acid as an efficient carrier for controlled anticancer drug delivery *J. Drug Deliv. Sci. Technol.* **44** 323–32
[21] Gholibegloo E, Mortezazadeh T, Salehian F, Forootanfar H, Firoozpour L, Foroumadi A, Ramazani A and Khoobi M 2019 Folic acid decorated magnetic nanosponge: an efficient nanosystem for targeted curcumin delivery and magnetic resonance imaging *J. Colloid. Interface Sci.* **556** 128–39
[22] Dramou P, Fizir M, Taleb A, Itatahine A, Dahiru N S, Mehdi Y A, Wei L, Zhang J and He H 2018 Folic acid-conjugated chitosan oligosaccharide-magnetic halloysite nanotubes as a delivery system for camptothecin *Carbohydr. Polym.* **197** 117–27
[23] Chen L, Zheng J, Du J, Yu S, Yang Y and Liu X 2019 Folic acid-conjugated magnetic ordered mesoporous carbon nanospheres for doxorubicin targeting delivery *Mater. Sci. Eng. C* **104** 109939
[24] Angelopoulou A, Kolokithas-Ntoukas A, Fytas C and Avgoustakis K 2019 Folic acid-functionalized, condensed magnetic nanoparticles for targeted delivery of doxorubicin to tumor cancer cells overexpressing the folate receptor *ACS Omega* **4** 22214–27
[25] Rosa M A *et al* 2024 Magnetic carbon nanotubes modified with proteins and hydrophilic monomers: cytocompatibility, *in-vitro* toxicity assays and permeation across biological interfaces *Int. J. Biol. Macromol.* **269** 131962
[26] Aydın B, Bozoğlu S, Karatepe N and Güner F S 2025 Synthesis of bovine serum albumin coated magnetic single walled carbon nanotubes as a delivery system for mitoxantrone *ACS Omega* **10** 102–13
[27] Lamanna G, Garofalo A, Popa G, Wilhelm C, Bégin-Colin S, Felder-Flesch D, Bianco A, Gazeau F and Ménard-Moyon C 2013 Endowing carbon nanotubes with superparamagnetic properties: applications for cell labeling, MRI cell tracking and magnetic manipulations *Nanoscale* **5** 4412–21
[28] Depan D, Shah J and Misra R D K 2011 Controlled release of drug from folate-decorated and graphene mediated drug delivery system: synthesis, loading efficiency, and drug release response *Mater. Sci. Eng. C* **31** 1305–12
[29] Ma N, Liu J, He W, Li Z, Luan Y, Song Y and Garg S 2017 Folic acid-grafted bovine serum albumin decorated graphene oxide: an efficient drug carrier for targeted cancer therapy *J. Colloid. Interface Sci.* **490** 598–607
[30] Wang Z, Zhou C, Xia J, Via B, Xia Y, Zhang F, Li Y and Xia L 2013 Fabrication and characterization of a triple functionalization of graphene oxide with Fe_3O_4, folic acid and doxorubicin as dual-targeted drug nanocarrier *Colloids Surf. B* **106** 60–65
[31] Erdem M, Yalcin S and Gunduz U 2017 Folic acid-conjugated polyethylene glycol-coated magnetic nanoparticles for doxorubicin delivery in cancer chemotherapy: preparation, characterization and cytotoxicity on HeLa cell line *Hum. Exp. Toxicol.* **36** 833–45
[32] Parın F N, Ullah S, Yıldırım K, Hashmi M and Kim I-S 2021 Fabrication and characterization of electrospun folic acid/hybrid fibers: *in vitro* controlled release study and cytocompatibility assays *Polymers* **13** 3594
[33] Zhang Y, Xing Y, Xian M, Shuang S and Dong C 2019 Folate-targeting and bovine serum albumin-gated mesoporous silica nanoparticles as a redox-responsive carrier for epirubicin release *New J. Chem.* **43** 2694–701
[34] Li J, Cai R, Kawazoe N and Chen G 2015 Facile preparation of albumin-stabilized gold nanostars for the targeted photothermal ablation of cancer cells *J. Mater. Chem. B* **3** 5806–14
[35] Ashuri A, Miralinaghi M and Moniri E 2022 Evaluation of folic acid-conjugated chitosan grafted Fe_3O_4/graphene oxide as a pH- and magnetic field-responsive system for adsorption and controlled release of gemcitabine *Korean J. Chem. Eng.* **39** 1880–90
[36] Nosrati H *et al*2022 Magnetite and bismuth sulfide Janus heterostructures as radiosensitizers for *in vivo* enhanced radiotherapy in breast cancer *Biomater. Adv.* **140** 213090
[37] Wang Y, Xu S, Xiong W, Pei Y, Li B and Chen Y 2016 Nanogels fabricated from bovine serum albumin and chitosan via self-assembly for delivery of anticancer drug *Colloids Surf. B* **146** 107–13
[38] Foroutan R, Peighambardoust S J, Latifi P, Ahmadi A, Alizadeh M and Ramavandi B 2021 Carbon nanotubes/β-cyclodextrin/$MnFe_2O_4$ as a magnetic nanocomposite powder for tetracycline antibiotic decontamination from different aqueous environments *J. Environ. Chem. Eng.* **9** 106344
[39] Han D, Zhang B, Su L and Yang B 2020 Attachment of streptavidin-modified superparamagnetic iron oxide nanoparticles to the PC-12 cell membrane *Biomed. Mater.* **15** 045014
[40] Peighambardoust S J, Mahdavi Z, Gholizadeh M, Foroutan R and Ramavandi B 2025 Pyrolytic carbon/Cloisite 30B/$ZnFe_2O_4$ as reclaimable magnetic nanocomposite for methylene blue decontamination *Colloids Surf. A* **704** 135543

[41] Habibizadeh M, Rostamizadeh K, Dalali N and Ramazani A 2017 Preparation and characterization of PEGylated multiwall carbon nanotubes as covalently conjugated and non-covalent drug carrier: a comparative study *Mater. Sci. Eng. C* **74** 1–9
[42] Liu Y, Guo L, Huang H, Dou J, Huang Q, Gan D, Chen J, Li Y, Zhang X and Wei Y 2019 Facile preparation of magnetic composites based on carbon nanotubes: utilization for removal of environmental pollutants *J. Colloid. Interface Sci.* **545** 8–15
[43] Zuo X, Wu C, Zhang W and Gao W 2018 Magnetic carbon nanotubes for self-regulating temperature hyperthermia *RSC Adv.* **8** 11997–2003
[44] Dinan N M, Atyabi F, Rouini M-R, Amini M, Golabchifar A-A and Dinarvand R 2014 Doxorubicin loaded folate-targeted carbon nanotubes: preparation, cellular internalization, *in vitro* cytotoxicity and disposition kinetic study in the isolated perfused rat liver *Mater. Sci. Eng. C* **39** 47–55
[45] Chen H, Zhang T, Zhou Z, Guan M, Wang J, Liu L and Zhang Q 2013 Enhanced uptake and cytotoxity of folate-conjugated mitoxantrone-loaded micelles via receptor up-regulation by dexamethasone *Int. J.Pharm.* **448** 142–9
[46] Hou L, Feng Q, Wang Y, Zhang H, Jiang G, Yang X, Ren J, Zhu X, Shi Y and Zhang Z 2015 Multifunctional nanosheets based on hyaluronic acid modified graphene oxide for tumor-targeting chemo-photothermal therapy *J. Nanopart. Res.* **17** 1–17
[47] Akinyelu J and Singh M 2019 Folate-tagged chitosan-functionalized gold nanoparticles for enhanced delivery of 5-fluorouracil to cancer cells *Appl. Nanosci.* **9** 7–17
[48] Akbar M U, Khattak S, Khan M I, Saddozai U A K, Ali N, AlAsmari A F, Zaheer M and Badar M 2023 A pH-responsive bi-MIL-88B MOF coated with folic acid-conjugated chitosan as a promising nanocarrier for targeted drug delivery of 5-Fluorouracil *Front. Pharmacol.* **14** 1–17
[49] Cao X T, Patil M P, Phan Q T, Le C M Q, Ahn B-H, Kim G-D and Lim K T 2020 Green and direct functionalization of poly (ethylene glycol) grafted polymers onto single walled carbon nanotubes: effective nanocarrier for doxorubicin delivery *J. Ind. Eng. Chem.* **83** 173–80
[50] Shi Z, Guo R, Li W, Zhang Y, Xue W, Tang Y and Zhang Y 2014 Nanoparticles of deoxycholic acid, polyethylene glycol and folic acid-modified chitosan for targeted delivery of doxorubicin *J. Mater. Sci. Mater. Med.* **25** 723–31
[51] Cole A J, Yang V C and David A E 2011 Cancer theranostics: the rise of targeted magnetic nanoparticles *Trends Biotechnol.* **29** 323–32
[52] Baneshi M, Dadfarnia S, Haji Shabani A M, Sabbagh S K and Bardania H 2022 AS1411 aptamer-functionalized graphene oxide-based nano-carrier for active-target and pH-sensitive delivery of curcumin *J. Iran. Chem. Soc.* **19** 2367–76
[53] Prajapati S K, Jain A, Shrivastava C and Jain A K 2019 Hyaluronic acid conjugated multi-walled carbon nanotubes for colon cancer targeting *Int. J. Biol. Macromol.* **123** 691–703
[54] Altuwaijri N and Atef E 2024 Transferrin-conjugated nanostructured lipid carriers for targeting artemisone to melanoma cells *Int. J. Mol. Sci.* **25** 9119
[55] Li X, Chen J, Liu H, Deng Z, Li J, Ren T, Huang L, Chen W, Yang Y and Zhong S 2019 β-Cyclodextrin coated and folic acid conjugated magnetic halloysite nanotubes for targeting and isolating of cancer cells *Colloids Surf. B* **181** 379–88
[56] Nosrati H, Sefidi N, Sharafi A, Danafar H and Kheiri Manjili H 2018 Bovine Serum Albumin (BSA) coated iron oxide magnetic nanoparticles as biocompatible carriers for curcumin-anticancer drug *Bioorg. Chem.* **76** 501–9
[57] Deb A and Vimala R 2018 Camptothecin loaded graphene oxide nanoparticle functionalized with polyethylene glycol and folic acid for anticancer drug delivery *J. Drug Deliv. Sci. Technol.* **43** 333–42
[58] Jawahar N, De A, Jubee S and Reddy E S 2020 Folic acid-conjugated raloxifene hydrochloride carbon nanotube for targeting breast cancer cells *Drug Dev. Res.* **81** 305–14
[59] Zhang X, Meng L, Lu Q, Fei Z and Dyson P J 2009 Targeted delivery and controlled release of doxorubicin to cancer cells using modified single wall carbon nanotubes *Biomaterials* **30** 6041–7
[60] Lu Y-J, Wei K-C, Ma C-C M, Yang S-Y and Chen J-P 2012 Dual targeted delivery of doxorubicin to cancer cells using folate-conjugated magnetic multi-walled carbon nanotubes *Colloids Surf. B* **89** 1–9